

HELIUM-LIKE TRIPLET DIAGNOSTICS

J. Dubau^{1,3} and D. Porquet^{2,3}

¹LSAI, U.M.R. 8624, CNRS, Université de Paris Sud, 91405 Orsay Cedex, France

²Service d'Astrophysique, CEA Saclay, 91191 Gif-sur-Yvette Cedex, France

³LUTH, F.R.E. 2462 CNRS, Observatoire de Paris, 92195 Meudon Cedex, France

ABSTRACT

The $1s^2$ – $1s2l$ lines are the most intense He-like ions lines. They are used as spectroscopic diagnostics for solar active regions as well as for different laboratory plasmas. Nowadays, it exists very high spectral resolution instruments and, for intense X-ray sources, one can do spectroscopic diagnostics from line ratios. With XMM (RGS) and Chandra (LETGS, HETGS) spectral resolutions and for several atomic elements, it is particularly possible to separate a 3 blended line set, the so-called He-like triplet: Resonance (r), Intercombination (i) and Forbidden (f), which are dominated respectively by lines issued from the following levels : $1s2p\ ^1P_1$, $1s2p\ ^3P_{1,2}$, and $1s2s\ ^3S_1$. We shall show that the measurement of two different ratios between these 3 lines ($R = f/i$ and $G = (f + i)/r$) give quantitative informations on the nature of the emitting plasma (photo-ionized or collisional) and on its electronic density and temperature. A more refined analysis must also include satellite line contributions.

Key words: atomic data – atomic process – line: formation – techniques: spectroscopic – X-rays

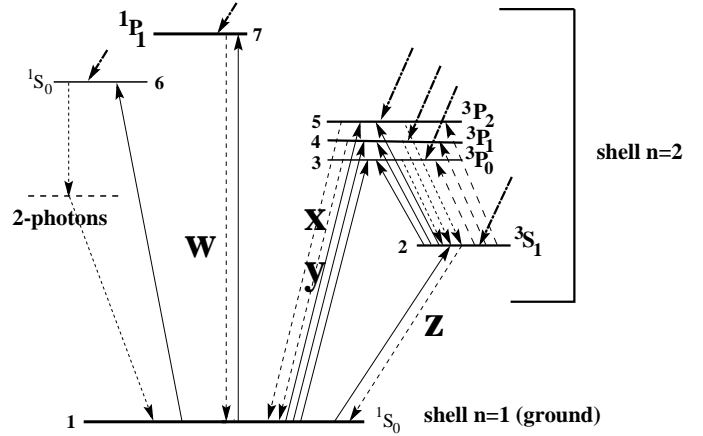


Figure 1. Simplified level scheme for Helium-like ions. **w** (or *r*), **x,y** (or *i*), and **z** (or *f*): resonance, intercombination, and forbidden lines, respectively. Full upward arrows: collisional excitation transitions, broken arrows: radiative transitions (including photo-excitation from 2^3S_1 to $2^3P_{0,1,2}$ levels, and 2-photon continuum from 2^1S_0 to the ground level), and thick skew arrows: recombination (radiative and dielectronic) plus cascade processes.

1. INTRODUCTION

In the X-ray range, the three most intense lines of Helium-like ions (“triplet”) are: the *resonance* line (*r*, also called *w*: $1s^2\ ^1S_0 - 1s2p\ ^1P_1$), the unresolved *intercombination* lines (*i*, also called *x + y*: $1s^2\ ^1S_0 - 1s2p\ ^3P_{2,1}$) and the *forbidden* line (*f*, also called *z*: $1s^2\ ^1S_0 - 1s2s\ ^3S_1$). They correspond to transitions between the $n=2$ shell and the $n=1$ ground-state shell (see Figure 1).

Gabriel & Jordan (1969) were the first to recognize that the ratios of these lines could give important plasma diagnostics on the electron density (n_e) and temperature (T_e).

$$R(n_e) = \frac{f}{i} \quad G(T_e) = \frac{f+i}{r} \quad (1)$$

These diagnostics have been used for coronal spectra as well as for many laboratory hot plasmas (e.g. tokamaks).

Helium-like spectral lines $1s^2$ – $1s2l$ have been observed with high spectral resolution for a long time in solar corona

X-ray spectra. During the seventies, several instruments have been flown aboard satellites to observe the soft X-ray spectra of solar flares. Spectra in the 1–25Å range, for example, have been obtained from uncollimated crystal spectrometers on the early OSO satellites (Neupert et al. 1973, Doschek et al. 1972), the OVI-17 satellite (Walker & Rugge 1970), and OSO 8 (Parkinson et al. 1978). Particular spectral regions (e.g. iron lines at 1.9Å) have been examined with the *intercosmos-4* spectrometer (Grineva et al. 1973) and the *SOLFLEX* instrument on the *P78-1* satellite (Doschek et al. 1979). Rocket-borne collimated crystal spectrometers have been recorded spectra in various ranges up to 25Å from active regions or weak flares (Parkinson 1975; Pye et al. 1977, Burek et al. 1981), while the collimated *SOLFLEX* instrument on *P78-1* has been obtained very high resolution spectra from sizable flares (McKenzie et al. 1980). Thanks to the Flat Crystal Spectrometer (FCS, Phillips et al. 1982) and Bent Crystal spectrometers (BCS, Culhane et al. 1981) on board the *Solar Maximum Mission* (SMM), many line blends were resolved for the first time allowing new physical information about the emitting plasma to be extracted. In particular the BCS

observed He-like iron and calcium. More recently Yohkoh (Solar A) contained also a BCS which pursued similar solar observations of iron and calcium as *SMM*, extending the observations to lower temperature by using Helium-like sulfur spectra (Harra-Murnion et al. 1996, Kato et al. 1997).

For active coronae and solar flares, a temporal analysis of these lines can be carried on during the three consecutive phases: ionization, gradual, recombination (e.g., Mewe & Schrijver 1978a, 1978b, 1978c; Doyle 1980; Pradhan & Shull 1981).

It is now possible, thanks to the spectral resolution of the new generation of X-ray satellites: Chandra and XMM-Newton, to resolve this triplet and to use these diagnostics in case of extra-solar objects. Indeed, the Helium-like “triplet” is a powerful tool in the analysis of high-resolution spectra of a variety of plasmas such as:

- collisional plasmas: e.g., *stellar coronae (OB stars, late type stars, active stars, ...)*
- photo-ionized or hybrid plasmas (photo-ionization + collisional ionization): e.g., *“Warm Absorber” (in AGNs), X-ray binaries, ...*
- out of equilibrium plasmas: e.g., *SNRs, stellar flares,*

The wavelength ranges of the RGS (6-35 Å), of the LETGS (2-175 Å), and of the HETGS (MEG range: 2.5-31 Å; HEG range: 1.2-15 Å) contain the Helium-like “triplets” from C V (or N VI for the RGS, and for the HETGS-HEG) to Si XIII (Table 1).

Table 1. Wavelengths in Å of the three main X-ray lines of C V, N VI, O VII, Ne IX, Mg XI and Si XIII (from Vainshtein & Safronova 1978).

label	line	C V	N VI	O VII	Ne IX	Mg XI	Si XIII
<i>r</i> (w)	<i>resonance</i>	40.279	28.792	21.603	13.447	9.1681	6.6471
<i>i</i> (x)	<i>inter-</i>	40.711	29.074	21.796	13.548	9.2267	6.6838
(y)	<i>combination</i>	40.714	29.076	21.799	13.551	9.2298	6.6869
<i>f</i> (z)	<i>forbidden</i>	41.464	29.531	22.095	13.697	9.3134	6.7394

These diagnostics have been recently used in numerous observations of extra-solar objects thanks to Chandra and XMM-Newton such as Active Galactic Nuclei (e.g., NGC 5548: Kaastra et al. 2000; NGC 4051: Collinge et al. 2001; MCG-6-30-15: Lee et al. 2001; NGC 4151: Ogle et al. 2000, Mrk 3: Sako et al. 2000; NGC 3783: Kaspi et al. 2000; Mkn 509: Pounds et al. 2001); stellar coronae and stellar winds (e.g., Vela X-1: Schulz et al. 2002; II Pegasi: Huenemoerder et al. 2001; Capella: Ness et al. 2001, Audard et al. 2001); and X-ray binaries (SS 433: Marshall et al. 2002; 4U 1626-67: Schulz et al. 2001; EXO 0748-67: Cottam et al. 2001). As an illustration, the spectra of He-

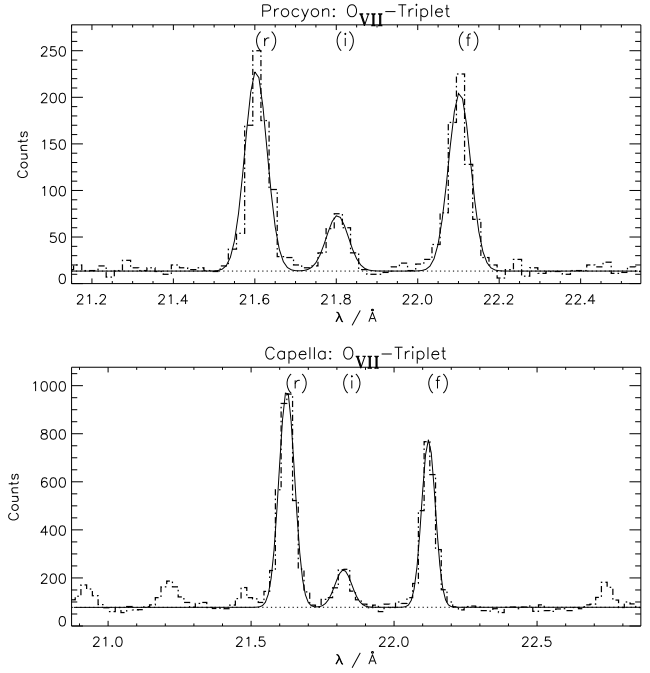


Figure 2. Observed spectra (Chandra, LETGS) of the He-like O VII triplet lines (*r*, *i*, and *f*) of the stellar coronae of Capella and Procyon (Ness et al. 2001).

like O VII ion of the stellar coronae of Capella and Procyon are shown in Figure 2.

They allow the determination of the ionization process (linked to the temperature) in case of the “Warm Absorber” in AGNs (photo-ionization and/or an additional ionization process such as shock or starburst). However, these diagnostics should be used cautiously in order to avoid any mistaken interpretation of the physical parameters of the observed plasmas. Indeed some neglected atomic processes can lead to wrong determination of the density and of the temperature and of the ionization processes: blended dielectronic satellite lines, photo-excitation due to a strong UV radiation field, resonant scattering (optical depth).

2. PLASMA DIAGNOSTICS

2.1. DENSITY DIAGNOSTIC

In the low-density limit, all $n=2$ states are populated directly or via upper-level radiative cascades by electron impact from the He-like ground state, by recombination (radiative and dielectronic) of H-like ions, and for $1s2s\ ^1S_0$ and 3S_1 levels, by collisional electron ionization from the $1s^22s\ ^2S_{1/2}$ lithium-like ground level (see Figure 3). This later is only important in the out of equilibrium ionization phase such as seen in solar flares (e.g., Mewe & Schrijver 1978a, 1978b, 1978c; Bely-Dubau 1982). If the suffix λ represents *f*, *i* and *r*, the line emissivity ϵ_λ can be written

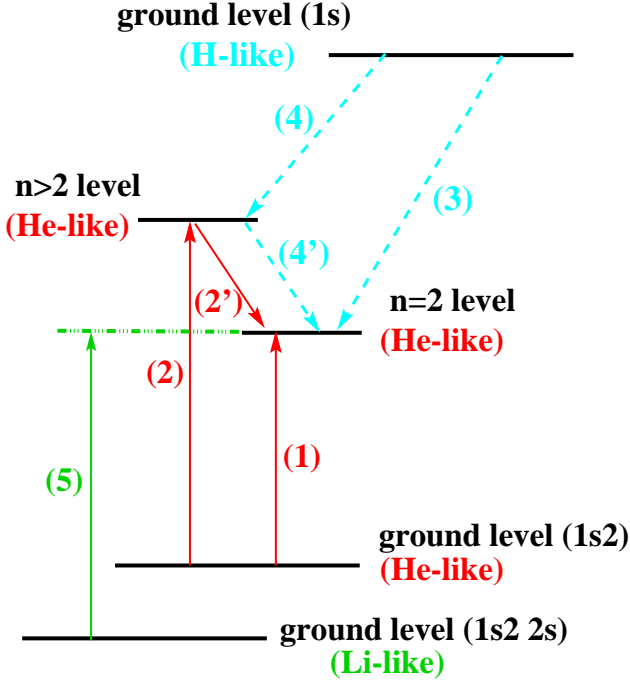


Figure 3. Simplified Grotrian diagram reporting the different contributions for the population of a given $n=2$ shell level. (1): direct contribution due to collisional excitation (CE) from the ground level ($1s^2$) of He-like ions; (2)+(2'): CE upper level radiative cascade contribution; (3): direct Radiative Recombination (RR) from H-like ions contribution; (4)+(4'): RR or Dielectronic Recombination (DR) upper level radiative cascade contribution; and (5): collisional ionization (CI) from the ground level ($1s^2 2s$) of Li-like ions. Note: CE, CI and DR are only important at high temperature. On the contrary, RR is important at low temperature.

as:

$$\epsilon_\lambda = n_e \left[C_\lambda^{He}(T_e) N(He - like) + C_\lambda^{Li}(T_e) N(Li - like) + \alpha_\lambda^H(T_e) N(H - like) \right]$$

Where C_λ^{He} , C_λ^{Li} , and α_λ^H are effective rate coefficients, i.e. including radiative cascades inside He-like levels, respectively excitation, ionization and recombination rates; and $N(He - like)$, $N(Li - like)$, and $N(H - like)$ are the population of $1s^2$, $1s^2 2s$ and $1s$ levels.

These $n=2$ levels decay radiatively directly or by cascades to the ground level. The relative intensities of the three intense lines are then independent of density. As n_e increases from the low-density limit, some of these states ($1s2s^3S_1$ and $1S_0$) are depleted by collisions to the nearby states where $n_{crit} C = A$, with C being the sum of the collisional rates depopulating the level, A being the radiative transition probability from $n=2$ to $n=1$ (ground state), and n_{crit} being the critical density. Collisional excitation depopulates first the $1s2s^3S_1$ level (upper level of the forbidden line) to the $1s2p^3P_{0,1,2}$ levels (upper levels of

the intercombination lines). The intensity of the forbidden line decreases while those of the intercombination lines increase, hence implying a reduction of the ratio R (according to Eq. 1), over approximately two or three decades of density (see Fig. 4).

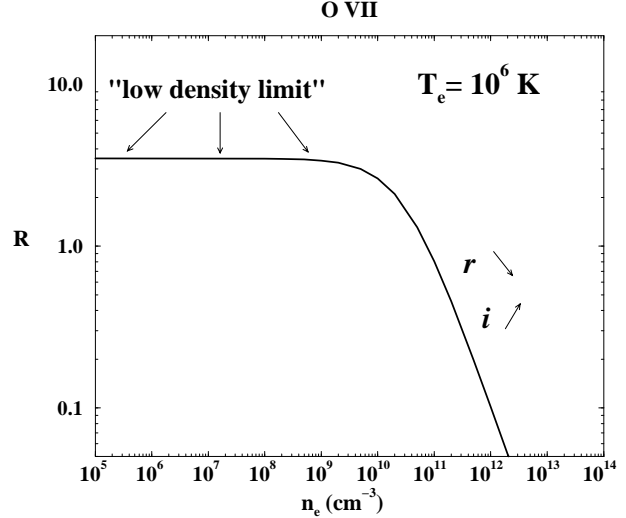


Figure 4. $R(n_e) = f/i$ for the He-like ion O VII in case of a collisional plasma. such as stellar coronae (calculations are taken from Porquet et al. 2001).

For much higher densities, $1s2s^1S_0$ is also depopulated to $1s2p^1P_1$, and the resonance line becomes sensitive to the density.

However caution should be taken for low-Z ions (i.e. C V, N VI, O VII) since in case of an intense UV radiation field, the photo-excitation between the 3S term and the 3P term is not negligible. This process has the same effect on the forbidden line and on the intercombination line as the collisional coupling, i.e. lowering of the ratio R , and thus could mimic a high-density plasma. It should be taken into account to avoid any misunderstanding between a high-density plasma and a high radiation field (see e.g. Porquet et al. 2001 for more details).

2.2. TEMPERATURE/IONIZATION PROCESS DIAGNOSTICS

The ratio G (see Eq. 1, and Fig. 5) is sensitive to the electron temperature since the collisional excitation rates have not the same dependence with temperature for the resonance line as for the forbidden and intercombination lines.

In addition, as detailed in Porquet & Dubau 2000 (see also Mewe 1999, and Liedahl 1999), the relative intensity of the resonance r line, compared to the forbidden f and the intercombination i lines, contains information about the ionization processes that occur: a strong resonance line compared to the forbidden or the intercombination lines corresponds to collision-dominated plasmas. It leads to a

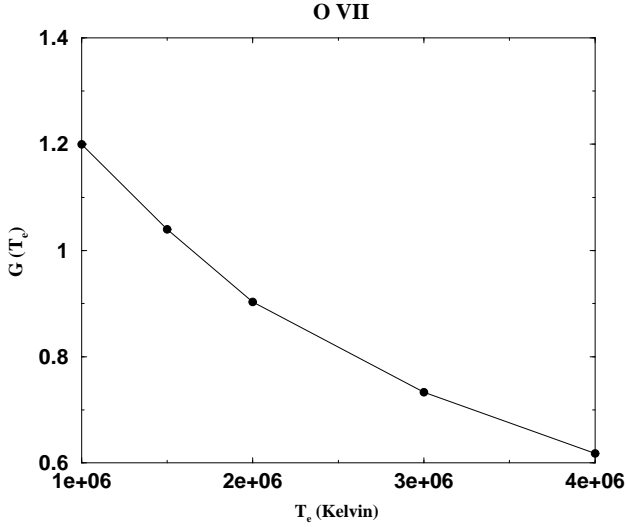


Figure 5. $G(T_e)$ for the He-like O VII in case of a collisional plasma, in the low density limit (calculations are taken from Porquet et al. 2001).

ratio of $G = (f + i)/r \sim 1$. On the contrary, a weak *resonance* line corresponds to plasmas dominated by photo-ionization ($G = (f + i)/r > 4$).

However, as mentioned for the density diagnostic, caution should be taken since photo-excitation can mimic a hybrid plasmas, i.e. photo-ionization plus collisional ionization, e.g. shock or starburst (see § 4).

3. NUMERICAL MODELING

3.1. ATOMIC DATA

Wavelengths and radiative probabilities: since 1930 many calculations using different approximations (simple methods up to relativistic many body methods). With the observed resolution of Chandra and XMM-Newton, a good agreement between these calculations can be reached easily, for example, for electron excitation rates see Dubau (1994).

3.2. BLENDED DIELECTRONIC SATELLITE LINES

The influence of the blending of dielectronic satellite lines for the *resonance*, the *intercombination* and the *forbidden* lines has been taken into account where their contribution is not negligible in the calculation of R and G , affecting the inferred electron temperature and density. This is the case for the high-Z ions produced in a collisional plasma, i.e. Ne IX, Mg XI, and Si XIII ($Z=10, 12$, and 14 , respectively).

$$R = \frac{f + satf}{i + sati} \quad (2)$$

$$G = \frac{(f + satf) + (i + sati)}{(r + satr)}, \quad (3)$$

where *satf*, *sati* and *satr* are respectively the contribution of blended dielectronic satellite lines to the *forbidden* line,

to the *intercombination* lines, and to the *resonance* line, respectively. One can note that at very high density the 3P levels are depleted to the 1P level, and in that case i decreases and R tends to *satf/sati*.

The intensity of a dielectronic satellite line arising from a doubly excited state with principal quantum number n in a Lithium-like ion produced by dielectronic recombination of a He-like ion is given by:

$$I_s = N_{He} n_e C_s, \quad (4)$$

where N_{He} is the population density of the considered He-like ion in the ground state $1s^2$ with statistical weight g_1 (for He-like ions $g_1 = 1$).

The rate coefficient (in $\text{cm}^3 \text{s}^{-1}$) for dielectronic recombination is given by (Bely-Dubau et al. 1979):

$$C_s = 2.0706 \cdot 10^{-16} \frac{e^{-E_s/kT_e}}{g_1 T_e^{3/2}} F_2(s), \quad (5)$$

where E_s is the energy of the upper level of the satellite line s with statistical weight g_s above the ground state of the He-like ion. T_e is the electron temperature in K, and $F_2(s)$ is the so-called line strength factor (often of the order of about 10^{13}s^{-1} for the stronger lines) given by

$$F_2(s) = \frac{g_s A_a A_r}{(\sum A_a + \sum A_r)}, \quad (6)$$

where A_a and A_r are transition probabilities (s^{-1}) by autoionization and radiation, and the summation is over all possible radiative and auto-ionization transitions from the satellite level s .

At the temperature at which the ion fraction is maximum for the He-like ion (see e.g. Mazzotta et al. 1998), the differences between the calculations for R (for G) with or without taking into account the blended dielectronic satellite lines are only of about 1% (9%), 2% (5%), and 5% (3%) for Ne IX, Mg XI, and Si XIII at the low-density limit and for $T_{rad}=0\text{K}$, respectively (see Porquet et al. 2001). At lower temperature, the contribution of the blended satellite lines become larger and at higher temperature it can be neglected.

For photo-ionized plasmas where recombination prevails and the temperature is much lower (e.g., $T \lesssim 0.1 T_m$), the effect on R and G can be much bigger since $I_{sat}/I_r \propto T^{-1} e^{(E_r - E_{sat})/kT}$. For very high density n_e the contribution of the blended dielectronic satellite lines to the forbidden line leads to a ratio R which tends to *satf/sati*, hence decreases much slower with n_e than in the case where the contribution of the blended DR satellites is not taken into account. The importance of the dielectronic satellite lines can be seen in the O VII He-like triplet spectra of Procyon on Figure 2, on the right hand side of r and the left hand side of f . They indicate a lower temperature coronal plasma compared to the Capella spectra.

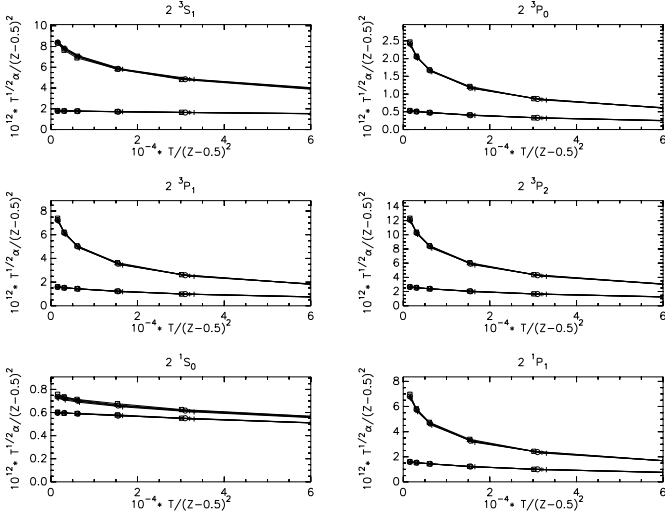


Figure 6. Scaled total radiative recombination rates (upper curves: direct plus cascade contribution from $n>2$ levels) $\alpha^s = T^{1/2} \alpha / (Z-0.5)^2$ ($\times 10^{12} \text{ cm}^3 \text{ s}^{-1}$) versus $T^s = T / (Z-0.5)^2$ ($\times 10^{-4}$) towards each $n=2$ level (Plus, star, circle and cross are respectively for $Z=8, 10, 12, 14$), and for comparison the direct contribution (lower curve in each graph). T is in Kelvin.

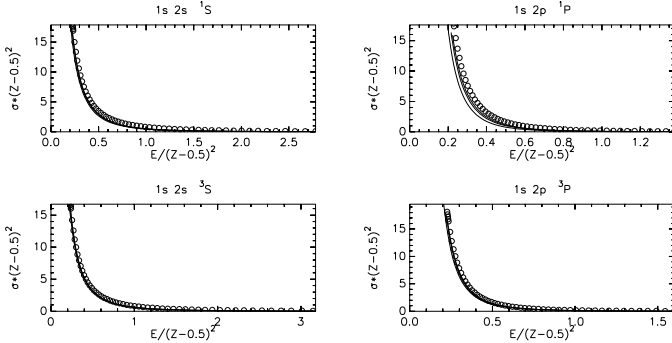


Figure 7. Scaled photoionization cross sections $\sigma_s = \sigma (Z-0.5)^2$ (in $\text{cm}^2 \text{ s}^{-1}$) as a function of $E/(Z-0.5)^2$ (E is in Rydberg). Empty circles: photo-ionization cross sections calculated in Porquet & Dubau (2000); solid lines: photo-ionization cross sections available in Topbase for different values of $Z=6, 10, 14$.

3.3. OPTICAL DEPTH

If the optical depth of the resonance line is not taken into account, the calculated ratio G could be overestimated (inferred temperature underestimated) when the optically-thin approximation is no longer valid. This has been estimated with an *escape-factor method*, e.g., for the case of a *Warm Absorber in an AGNs* (Porquet, Kaastra, Mewe, Dubau 2002).

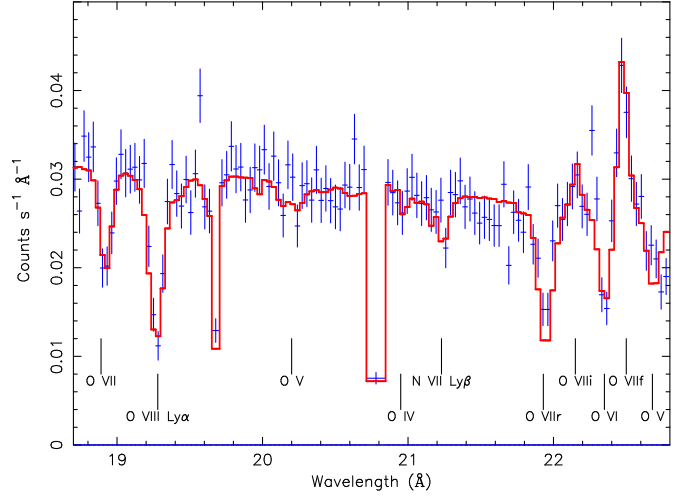


Figure 8. X-ray spectra (XMM-Newton, RGS) of the energy range containing the He-like O VII triplet (r , i , and f lines) showing also the photo-absorbed lines of $\text{Ly}\alpha$ (O VIII), r (O VII) as well two satellite lines q (O VI) and β (O V) (Steenbrugge et al. 2002).

4. PHOTO-IONIZED MODEL

“Warm Absorbers” in AGN are typical examples of photo-ionized (PI) plasmas which are dominantly ionized by an intense radiative source, in such plasmas the electron temperature is relatively small. Then atomic levels are predominantly populated by direct (radiative and/or dielectronic) recombination or by radiative cascades from upper levels, which are very important data. For the modeling of such plasmas the atomic data required are the radiative probabilities, the radiative and dielectronic recombination rates to individual levels, $1s n l^S L_J$, with $n \leq 10$, plus extrapolation of n to infinity. Such a large basis of ionic states is necessary because the radiative recombination is slowly convergent with n .

The cascade contribution of radiative contribution is very important for small temperature, as it can be seen in Figure 6. In Figure 7 the comparison of two different calculations for radiative recombination is done:

- (1) TOPBASE, a very sophisticated calculation using the R-matrix code;
- (2) screened hydrogenic data obtained from analytical quantum expression. It is interesting to see in Figures 6 and 7 that the data can be easily scaled along the iso-electronic sequence ($Z=8, 10, 12, 14$: Porquet & Dubau 2000).

As detailed above the electron density diagnostic is due to the electron excitation inside the $n=2$ levels. However to get reliable diagnostics, photo-excitation between these close-levels must also be accounted for.

Recently, Kinkhabwala et al. (2002), pointed out also the important effect of the photo-excitation in the high Rydberg series lines. Indeed, the ratio of high- n lines to $\text{Ly}\alpha$ bring evidence for photo-excitation in Warm Absorber Seyfert 2. They clearly showed that in addition to

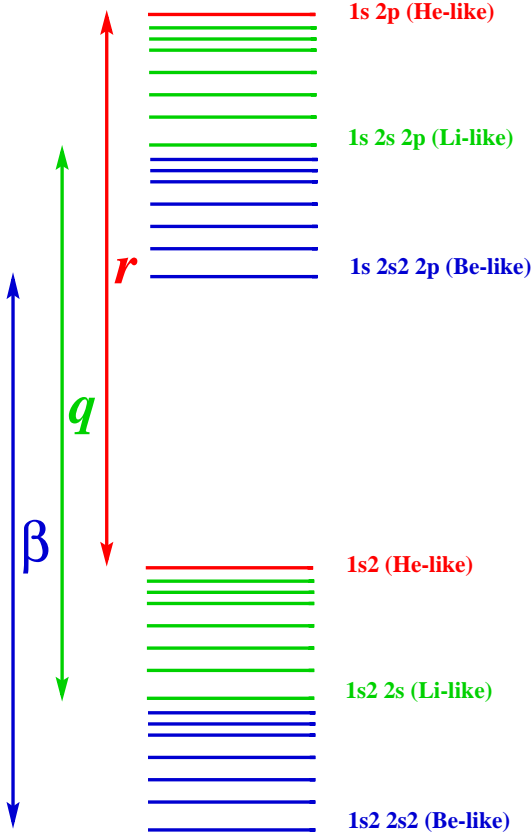


Figure 9. Energy level diagram showing the parent resonance line r in the Helium-like ion together with two strong satellite lines due to photo-absorption: q in Li-like, β in Be-like.

photo-ionization (treated in Porquet & Dubau 2000), photo-excitation process is sufficient to fit the data of Seyfert galaxies without needing an additional collisional ionization process (e.g. shock or starburst). Then both photo-ionization and photo-excitation are needed to infer unambiguously the ionization process occurring in the plasmas.

In Figure 8 is shown an interesting photo-ionized plasma spectrum of O VII and O VIII obtained by XMM-Newton RGS for NGC 5548 (Steenbrugge et al. 2002). On this spectra one can see photo-absorbed lines of Ly- α (O VIII), r (O VII) as well two satellite lines q (O VI) and β (O V). On the contrary, the f and i lines are seen as expected in emission, they are probably due to recombination of H-like ion (here O VIII). The two satellite lines q and β are located respectively between between O VII i and f , and on the right hand side of f . An energy level diagram is shown in Figure 9, it explains why the q and β lines are satellites of r , i.e. have very close in wavelength to r . We can also notice that the upper levels of q and β can auto-ionize since they are above $1s^2$: $1s2s2p$ decays to $1s^2$ and $1s2s^22p$ decays preferably to $1s^22s$ and $1s^22p$.

5. COLLISIONAL AND HYBRID MODELS

In pure collisional model, atoms are ionized by electron collision, the free electrons being heated by some external source. Electron collision is the dominant excitation process, and spontaneous emission is the dominant de-excitation process.

A hybrid model is a mixing of both collisional and photo-ionized models.

A strong radiation field can mimic a high density if the photo-excitation 3S_1 level (f line) \rightarrow $^3P_{0,1,2}$ levels (i lines) exceeds the electron collisional excitation. ex: ζ Puppis (Kahn et al. 2001, Cassinelli et al. 2001). Rate of photo-excitation (in s^{-1}) (Mewe & Schrijver 1978a) in a stellar photospheric radiation field with effective black-body radiation temperature T_{rad} is written as:

$$B_{mp_k} = \frac{W A_{p_k m} (w_{p_k} / w_m)}{\exp\left(\frac{\Delta E_{mp_k}}{k T_{rad}}\right) - 1}, \quad (7)$$

where A and B are the Einstein coefficients and the radiation is diluted by a factor W given by

$$W = \frac{1}{2} \left[1 - \left(1 - \left(\frac{r_*}{r} \right) \right)^{1/2} \right], \quad (8)$$

- $W=1/2$ (close to the stellar surface, $r = r_*$; e.g., Capella and Procyon: Audard et al. 2001, Mewe et al. 2001, Ness et al. 2001).

- $W \ll 1/2$ (radiation originates from another star at larger distance; e.g., Algol, where K-star is irradiated by B-star, $W \simeq 0.01$: Ness et al. 2002).

Porquet et al. (2001) showed that photo-excitation is important for C V, N VI, O VII for $T_{rad} \geq (5-10) 10^3$ K (see Fig. 3 in Porquet et al. 2002), and for higher-Z ions when $T_{rad} \geq \text{few } 10^4$ K.

6. LABORATORY SPECTRA

Helium-like lines are now currently observed in many laboratory plasmas: tokamaks (e.g., Doyle & Schwob 1982), laser produced plasmas (e.g., Renaudin et al. 1994), Z-pinch (e.g., Coulter et al. 1988). The former diagnostics have often been used.

Atomic data can be checked by comparison with laboratory measurements, ions being produced by ionic sources: EBIT (Wargelin et al. 2001).

7. CONCLUSION

We have shown that the ratios of the three main lines (forbidden, intercombination and resonance) of He-like ions provide very powerful diagnostics for totally or partially photo-ionized media. For the first time, these diagnostics can be applied to non-solar plasmas thanks to the high spectral resolution and the high sensitivity of the new X-ray satellites *Chandra*, and *XMM-Newton*:

- collisional plasmas: e.g., stellar coronae (OB stars, late

type stars, active stars, ...);

- photo-ionized or hybrid plasmas (photo-ionization + collisional ionization):
e.g., “Warm Absorber” (in AGNs), X-ray binaries, ...
- out of equilibrium plasmas: *e.g., SNRs, stellar flares,*

These diagnostics have strong advantages. The lines are emitted by the same ionization stage of one element, thus eliminating any uncertainties due to elemental abundances. In addition, since the line energies are relatively close together, this minimizes wavelength dependent instrumental calibration uncertainties, thus ensuring that observed photon count rates can be used almost directly.

These diagnostics should be used not as stand-alone one but should be used combined to other plasma diagnostics such as those based on radiative recombination continuum (RRC; Liedahl & Paerels 1996), Fe-L shell lines (see review of Liedahl et al. 1992), which give respectively indication on the ionization process as well as on the density.

In a close future high spectral resolution spectra at higher energy range (Astro-E2, Constellation-X, XEUS) will give access to higher Z He-like ions such as sulfur, calcium and iron, which are sensitive to higher range of density and temperature.

ACKNOWLEDGEMENTS

D.P. acknowledges grant support from the “Institut National des Sciences de l’Univers” and from the “Centre National d’Etudes Spatial” (France).

REFERENCES

- Audard, M., Behar, E., Güdel, M., Raassen, A. J. J., Porquet, D., Mewe, R., Foley, C. R., Bromage, G. E. (2001), *A&A*, 365, L329
- Bely-Dubau, F., Gabriel, A. H., Volonté, S. (1979), *MNRAS*, 189, 801
- Bely-Dubau F., Dubau J., Faucher P., Gabriel A. H. (1982), *MNRAS*, 198, 239
- Burek A. J., Barrus D. M., Blake R. L., Fenimore E. E. (1981), *ApJ*, 243, 660
- Cassinelli J. P., Miller N. A., Waldron W. L., MacFarlane J. J., Cohen D. H. (2001), *ApJ*, 554, L55
- Collinge M. J., Brandt W. N., Kaspi S., Crenshaw, D. M., Elvis, M., Kraemer, S. B., Reynolds, C. S., Sambruna, R. M., Wills, Beverley J. (2001), *ApJ*, 557, 2
- Cottam J., Kahn S. M., Brinkman A. C., den Herder J. W., Erd C. (2001), *A&A*, 365, L277
- Coulter M. C., Apruzese J. P., Kepple P. C. (1988), *Journal of Applied Physics*, 63, 2221
- Culhane J. L., Rapley C. G., Bentley R. D., Gabriel, A. H., Phillips, K. J., Acton, L. W., Wolfson, C. J., Catura, R. C., Jordan, C., Antonucci, E. (1981), *ApJ*, 244, L141
- Doyle J.G. (1980), *A&A*, 87, 183
- Doyle J. G., Schwob J. L., 1982, *Journal of Physics B Atomic Molecular Physics*, 15, 813
- Doschek G. A., Meekins J. F., Cowan R. D. (1972), *ApJ*, 177, 261
- Doschek G. A., Kreplin R. W., Feldman U. (1979), *ApJ*, 233, L157
- Dubau J. (1994), *Atomic Data and Nuclear Data Tables*, 57, 21
- Gabriel A.H. & Jordan, C. (1969), *MNRAS*, 145, 241
- Grineva Y. I., Karev V. I. K. V. V., Krutov V. V., Mandelstam S. L., Vainstein L. A., Vasilyev B. N., Zhitnik I. A. (1973), *Solar Physics*, 29, 441
- Harra-Murnion, L. K., Phillips, K. J. H., Lemen, J. R., Zarro, D. M., Greer, C. J., Foster, V. J., Barnsley, R., Coffey, I. H., Dubau, J., Keenan, F. P., Fludra, A., Rachlew-Kaellne, E., Watanabe, T., Wilson, M. (1996), *A&A* 308, 670-684
- Huenemoerder D. P., Canizares C. R., Schulz N. S. (2001), *ApJ*, 559, 1135
- Kaastra J. S., Mewe R., Liedahl D. A., Komossa S., Brinkman A. C. (2000), *A&A*, 354, L83
- Kaastra J. S., Mewe R., Porquet D., Raassen A. J. J. (2002), in preparation (Paper IV)
- Kahn S. M., Leutenegger, M. A., Cottam, J., Rauw, G., Vreux, J.-M., den Bogende, A. J. F., Mewe, R., Güdel, M. (2001), *A&A*, 365, L312
- Kaspi S., Brandt W. N., Netzer H., Sambruna R., Chartas G., Garmire G. P., Nousek J. A. (2000), *ApJ*, 535, L17
- Kato T., Safronova U., Shlyptseva A., Cornille M., Dubau J., Nilsen J., 1997, *Atomic Data and Nuclear Data Tables*, 67, 225
- Kinkhabwala et al. (2002), these proceedings
- Lee J. C., Ogle P. M., Canizares C. R., Marshall H. L., Schulz N. S., Morales R., Fabian A. C., Iwasawa K. (2001), *ApJ*, 554, L13
- Liedahl D. A., Kahn S. M., Osterheld A. L., Goldstein W. H., 1992, *ApJ*, 391, 306
- Liedahl, D. A., Paerels, F. (1996), *ApJ*, 468, 33
- Liedahl D. A. (1999), *X-Ray Spectroscopy in Astrophysics*, 189
- Marshall H. L., Canizares C. R., Schulz N. S. (2002), *ApJ*, 564, 941
- Mazzotta P., Mazzitelli, G., Colafrancesco, S., Vittorio, N. (1998), *A&AS*, 133, 403
- Mauche C. W., Liedahl D. A., Fournier K. B., 2001, *ApJ*, 560, 992
- McKenzie D. L., Landecker P. B., Broussard R. M., Rugge H. R., Young R. M., Feldman U., Doschek G. A. (1980), *ApJ*, 241, 409
- Mewe R. & Schrijver J. (1978a), *A&A*, 65, 99
- Mewe R. & Schrijver J. (1978b), *A&A*, 65, 115
- Mewe R. & Schrijver J. (1978c), *A&AS*, 45, 11
- Mewe R. (1999), *X-Ray Spectroscopy in Astrophysics*, 109
- Mewe R., Raassen A.J.J., Drake J.J., Kaastra J.S., van der Meer R.L.J., Porquet D. (2001), *A&A*, 368, 888
- Mewe R. (2002), these proceedings
- Ness J.-U., Mewe R., Schmitt J.H.M.M., Raassen A.J.J., Porquet D., Kaastra, J. S., van der Meer, R. L. J., Burwitz, V., Predehl, P. (2001), *A&A*, 367, 282
- Ness J.-U. et al. (2002), in preparation
- Neupert W. M., Swartz M., Kastner S. O. (1973), *Solar physics*, 31, 171
- Ogle P. M., Marshall H. L., Lee J. C., Canizares C. R. (2000), *ApJ*, 545, L81
- Parkinson J. H. (1975), *Solar physics*, 42, 183

- Parkinson J. H., Wolff R. S., Kestenbaum H. L., Ku, W. H.-M., Lemen, J. R., Long, K. S., Novick, R., Suozzo, R. J., Weisskopf, M. C. (1978), *Solar physics*, 60, 123
- Phillips K. J. H., Fawcett B. C., Kent B. J., Gabriel, A. H., Leibacher, J. W., Wolfson, C. J., Acton, L. W., Parkinson, J. H., Culhane, J. L., Mason, H. E. (1982), *ApJ*, 256, 774
- Porquet D. & Dubau J. (2000), *A&AS*, 143, 495 (Paper I)
- Porquet D., Mewe R., Dubau J., Raassen A. J. J., Kaastra J. S (2001), *A&A*, 376, 1113 (Paper II)
- Porquet D., Kaastra J. S, Mewe R., Dubau J. (2002), in preparation (Paper III)
- Pounds K., Reeves J., O'Brien P., Page K., Turner M., Nayakshin S. (2001), *ApJ*, 559, 181
- Pradhan A. K. & Shull J. M. (1981), *ApJ*, 249, 821
- Pye J. P., Evans K. D., Hutcheon R. J. (1977), *MNRAS*, 178, 611
- Renaudin P., Chenais-Popovics C., Gauthier J. C., Peyrusse O., Back C. A. (1994), *Physical Review E*, 50, 2186
- Sako M., Kahn S. M., Paerels F., Liedahl D. A. (2000), *ApJ*, 543, L115
- Schulz N. S., Chakrabarty D., Marshall H. L., Canizares C. R., Lee J. C., Houck J. (2001), *ApJ*, 563, 941
- Schulz N. S., Canizares C. R., Lee J. C., Sako M. (2002), *ApJ*, 564, L21
- Steenbrugge, J. S. Kaastra, A. C. Brinkman, R. Edelson (2002), these proceedings
- Vainshtein L. A., Safronova U. I. (1978), *Atomic Data and Nuclear Data Tables*, 21, 49
- Walker A. B. C., Ruge H. R. (1970), *A&A*, 5, 4
- Wargelin B. J., Kahn S. M., Beiersdorfer P., 2001, *Phys. Rev. A*, 63, 2710